Prediction of airblast loads on structures behind a protective barrier

X. Q. Zhou and H. Hao*

School of Civil & Resource Engineering, the University of Western Australia,

35 Stirling Highway, Crawley WA 6009, Australia

Abstract

Experimental results and numerical simulations have demonstrated that a protective barrier can effectively reduce blast load and therefore protect structures from an external explosion. However, there are no formulae in the open literature that can be used to estimate the blast loads on a structure behind a barrier. In this paper, pseudo-analytical formulae based on numerical results are derived to estimate the reflected pressure-time history on a rigid wall behind a protective barrier. Numerical simulations of blast wave propagation are carried out to estimate the peak reflected pressure and the impulse on a rigid wall behind a blast barrier. The shock wave front arrival time and positive phase duration are extracted from the numerical results. Pseudo-analytical formulae, which are derived from the best-fitted curves of the numerical results, are suggested. These formulae can be used with those given in TM5-1300 or other methods for blast pressure estimation in the no-barrier case, to estimate pressure-time histories at various building locations behind a protective barrier.

Keywords: Blast loading; Protective barrier; Numerical simulation; Pressure-time history; Impulse

1. Introduction

Accidental or intentional explosion events often damage structures and injure occupants. Terrorist bombing that have occurred in the past few years have greatly heightened the awareness of structural

* Corresponding author. Tel.: +61-8-6488-1825; fax: +61-8-6488-1044.
E-mail address: hao@civil.uwa.edu.au (H. Hao)

engineers of the threat of terrorist attack using explosive devices. Blast loading has received considerable attention in recent years. Much research has been done to estimate the blast loading and analyze blast effects on structures [1-4]. Protecting civilian buildings from the threat of terrorist activities has also become one of the most critical challenges for researchers today. Some critical infrastructures, such as embassies, government buildings and power plants, need be carefully designed or retrofitted to resist blast loading and protect occupants because they might be potential terrorist targets. One simple way of enhancing the survivability of these structures to blast loads is to provide a blast barrier, or blast wall, at the perimeter [5]. A blast wall provides a stand-off distance to protect the structure from an external explosion. Moreover, it acts as an obstacle in the direction of the blast wave propagation. Therefore, some portion of the explosive energy is reflected back, and then the distribution of the blast pressure on the structure behind the barrier is changed and the peak pressure is reduced.

Both experimental and numerical results have demonstrated that a blast wall can effectively protect buildings from external explosion [5–9]. Rose et al. [5, 6] measured the blast environment behind a blast wall in scaled tests and developed comprehensive contour plots of overpressure and impulse behind the wall. Blast walls of different materials were tested in their later work in [7] and it was found that non-permanent structures could also result in a high degree of blast wave attenuation. Bogosian and Piepenburg [8] also analysed some experimental results to study the effectiveness of frangible barriers for blast shielding. Ngo et al. [9] presented some parametric studies on the effectiveness of barrier walls for a range of stand-off distances and wall heights. The authors [10] have derived some approximate formulae to predict maximum reflected pressure and the impulse on a building behind a blast wall. However, there is no direct method that can be employed to estimate the pressure-time history on structures if there exists a blast wall between the explosive centre and the structure. On the other hand, there are many empirical formulae and design charts available in the literature to estimate the blast loading on a structure when there is no barrier, such as TM5-1300 [11] and Henrych's empirical formulae [12]. The objective of the present paper is to derive pseudo-analytical formulae for an easy estimation of the blast loading, i.e., reflected pressure-time histories, on structures behind a protective barrier.

Previously, empirical formulae were mainly derived from blast experimental results. However, explosion tests are not only very expensive but also not possible in many cases due to safety and

environmental considerations. With the development of computer technology and computational mechanics, it becomes possible to reliably predict airblast loading on structures with numerical techniques. In particular, some wave propagation codes, termed 'hydrocodes', such as AUTODYN, have been proven to give reliable prediction of shock wave propagation and blast loading [1, 13, 14], and are available as commercial software. AUTODYN3D is employed in the present study to carry out the numerical analyses of blast wave propagation and to estimate blast pressure-time histories on structures behind a blast barrier. Pseudo-analytical formulae are derived from the best fitted curves of the numerical results for predictions of blast loading on structures behind a blast barrier.

The derived formulae are presented in terms of the critical parameters that affect the blast loading behind a blast wall, namely, the TNT equivalent charge weight W, the distance from charge to the building D, the height of the building H_B, the height of the gauge point on the structure H, the blast wall height H_1 and the ratio of the distance between the blast wall and the explosion to that between the building and the explosion L_1/D, as shown in Figure 1. It should be noted that in this study only surface explosion is considered, and the thickness of the blast wall is assumed to be 250 mm. Based on numerical results, the peak reflected pressure, the positive impulse, the shock wave front arrival time and the positive phase duration have been extracted to construct the pseudo-analytical formulae for estimating pressure-time histories on structures behind a blast wall. Approximate triangular form pressure-time history similar to that suggested in TM5-1300 is adopted in the present study.

2. Numerical Simulation

AUTODYN3D is a general-purpose three-dimensional software package that uses finite difference, finite volume, and finite element techniques to solve non-linear problems in solid, fluid and gas dynamics. It is particularly suited to the modelling of impact, penetration, blast and explosion events. The accuracy of using AUTODYN3D in predicting blast wave propagation has been proven [1, 3, 15]. Therefore, it is employed in the present study.

2.1 Material Model

In the simulation, both the blast wall and the building structure are assumed to be rigid; air and high explosive (TNT) are modelled by an Euler processor with equations of state being idea gas and Jones-

Wilkins-Lee (JWL), respectively. It should be noted that the assumption of a rigid blast wall and building structure in the simulation may lead to some inaccurate estimation of blast load on the structure. For example, interaction between the blast wave and a flexible structure may slightly reduce the blast load on the structure. Also blast load may destroy the blast wall when it is close to the explosion centre and generate fragment impact on the structure from debris. These effects are not considered in the present numerical simulation, as the primary objective of the study it to derive pseudo-analytical formulae for an estimation of the blast loads on structures behind a blast barrier. Modelling the secondary debris impact on structures owing to the damage of blast wall is very important as fragments maybe the primary source of casualties. This, however, will be the subject of further studies.

In the numerical model, air is modeled by an ideal gas equation of state, which is one of the simplest forms of equation of state. The pressure is related to the energy by

$$p = (\gamma - 1)\rho e \tag{1}$$

where γ is a constant, ρ is air density and e is the specific internal energy. In the simulation, the standard constants of air from AUTODYN material library are used, that is, air density, $\rho = 1.225 kg/m^3$ and $\gamma = 1.4$. The air initial internal energy is assumed to be $2.068 \times 10^5 kJ/kg$.

High explosives are typically modelled by using the Jones-Wilkins-Lee (JWL) equation of state, which models the pressure generated by chemical energy in an explosion. It can be written in the form,

$$p = C_1\left(1 - \frac{\omega}{r_1 v}\right)e^{-r_1 v} + C_2\left(1 - \frac{\omega}{r_2 v}\right)e^{-r_2 v} + \frac{\omega e}{v} \tag{2}$$

where p = hydrostatic pressure; v = specific volume; e = specific internal energy; and C_1, r_1, C_2, r_2 and ω are material constants. The values of the constants for many common explosives have been determined from dynamic experiments and are available in AUTODYN [16]. In the present simulation, C_1, r_1, C_2, r_2, and ω are assumed as, 3.7377×10^5MPa, 4.15, 3.7471×10^3MPa, 0.9 and 0.35 respectively.

2.2 Problem Setup

The dimensions of the present problem are shown in Figure 1. The TNT charge is assumed to be hemispherical and located at the ground level. The TNT charge weight W used in the simulations is,

respectively, 10kg, 30kg, 100kg, 300kg, 1000kg, 3000kg, 5000kg and 10000kg. The height of the building H_B varies from 3m to 40m, the distance between the charge and the building, D, varies from 5m to 50m, the height of the blast wall H_1 ranges from 1m to 4m. The ratio of the distance between the blast wall and the explosion to that between the building and the explosion L_1/D is from 0.2 to 0.8, i.e., L_1 varies from 1m to 40m. The effect of the barrier thickness was studied by varying the thickness from 150 mm to 300 mm in the numerical simulations. It was found that over this common barrier thickness range, varying the barrier thickness causes only insignificant changes in the blast loads on the structures behind the barrier. Therefore, hereafter, only the results with the barrier thickness of 250 mm are presented. The width of the barrier and the structure are assumed to be infinitely long. However, only 20m is considered in the 3D model because further increase in the width of the barrier has negligible effect on blast load along the center symmetric line of the structure. It should be noted that only half of the barrier and structure is included in the model owing to symmetry. Therefore the model implies a 40m long barrier and structure.

The numerical simulation is divided into two stages: in the first stage the initial detonation and propagation of the hemi-spherical blast wave are modelled in a 2D axial symmetric simulation; then in the second stage the results from the 2D calculation are remapped to a 3D simulation. Compared with a full 3D model, the number of cells required in a 2D model to produce accurate solutions is a lot less. Before the blast wave interacts with the rigid wall, the surface explosion can be modelled by an axially symmetric 2D model. When the blast wave begins to interact with the wall it becomes three-dimensional. Therefore, 3D simulation has to be used. This procedure not only reduces the time required for a calculation but also increases its accuracy due to the fine 2D mesh resolution in the initial high explosive detonation and expansion phases [17].

2.3 Model calibration

To study the mesh sensitivity and calibrate the accuracy of the numerical results, two different element sizes, namely, 500mm and 250mm for the 3D model are considered in the present study. As for the initial 2D model, a mesh size of 10 mm was used and which was proven yielding accurate predictions of shock wave propagation [17]. Because only the blast pressure and impulse for the no barrier case are available in the literature (such as in TM5-1300), only the no barrier case is considered for model

calibration. Figure 2 shows the comparison of the numerical results and the prediction from TM5-1300 for the maximum peak reflected pressure and the impulse at different scaled distances ($Z=D/W^{1/3}$) when $H_B=20m$, $D=20m$. Figure 3 shows the comparison of the peak reflected pressure and the impulse along the building height when $H_B=20m$, $D=20m$ and $W=1000kg$. As shown in both figures, there is a difference of up to -37.5% between the numerical peak pressures for element size of 250mm and the empirical results. When the mesh size is 500mm, the error can be as high as -58%. However, the impulse agrees well with the empirical results. These observations indicate that the numerical model fails to capture the very sharp peak of the blast wave. Further reducing the element size will result in a better estimation of peak pressures, but substantially increase the computational time and caused computer memory overflow. Convergence tests for the cases with a barrier between the explosion and building were also performed. It was found that the largest difference between the estimated peak pressure for mesh size 250 mm and 500 mm is about 28%. Because of the limitation of the computer and software capacity, further reducing the mesh size was not possible. Since a very sharp peak pressure has little effect on structures, and using the mesh size of 250 mm gave a very good estimation of impulses, the mesh size of 250 mm is used in the present study to carry out the numerical simulations. The maximum error owing to insufficiently small mesh size is up to 37.5% for peak reflected pressure, but the estimated impulse agrees well with those from TM5-1300.

2.4 Typical wave propagation results

More than 800 cases were calculated in the present study. Only some typical results are shown in this section. Figure 4 shows airblast pressure wave propagation when $H_B=20m$, $H_1=4m$, $D=20m$, $W=1000kg$, $L_1/D=0.6$. In this Figure, the reflection of the blast wave can be clearly seen.

Figure 5 shows the comparison of the reflected pressure time history at two different gauge points for the no barrier case and the with barrier case. From this figure, it can be seen that: (1) not only the peak reflected pressure is reduced but also the arrival time is delayed when there is a barrier; (2) the time delay caused by the barrier is longer when the gauge point height H is lower; (3) the duration of the positive phase for the with barrier case is longer than that for the no barrier case; (4) there may be two pulses due to the blast reflection (Figure 5b); (When the reflected blast wave from the front of the building reaches the back of the barrier, it will be reflected by the back surface and propagates again to the building,

causing the second pulse.) (5) the peak pressure, impulse and the duration in the negative phase for that with and without barrier case are nearly the same. Therefore, the negative phase can be assumed to be the same as that in the no barrier case. The positive phase is the main concern of the present study. It should be noted that, as shown in Figure 5, the simulated blast wave time-histories have a rather prominent rise time. This may be caused owing to insufficiently small mesh size used in the simulation. Since most recorded blast wave time-histories display a very sharp rise from ambient pressure to the peak pressure, and rise time becomes prominent only when the stand-off distance is relatively large, in this study the rise time is assumed to be zero. This assumption is consistent with most available empirical relations used in blast analysis and design, such as TM5-1300.

3 Analysis of Peak Pressure and Impulse

To allow for an easy estimation of blast pressure and impulse on structures behind a barrier, two modification factors for peak reflected pressure A_p and for impulse A_i are introduced. They are defined as the ratio of the peak reflected pressure and the ratio of the positive impulse on a building surface estimated with and without a blast wall in front of the building, respectively. That is, $A_p=P_{with\_barrier}/P_{no\_barrier}$, $A_i=I_{with\_barrier}/I_{no\_barrier}$, where $P_{no\_barrier}$ and $I_{no\_barrier}$ are the maximum pressure and impulse at the ground level on the building surface for the no barrier case, respectively. These modification factors, together with other available empirical methods such as TM5-1300 [11] obtained without a blast wall between the explosive and the structure, facilitate an easy estimation of the peak reflected pressure and impulse on structures behind a blast wall.

3.1 Peak reflected pressure and impulse distribution

In the simulation, both the maximum reflected pressure and the impulse are calculated. Comparisons of the peak reflected pressure distribution and the impulse distribution over the height of the building with and without a blast wall are shown in Figure 6. In the figure, $H_B=20m$, $H_1=2.5m$, $D=20m$, $W=1000kg$, L_1/D varies from 0.2 to 0.8 to show its effect on the pressure and impulse distribution. The vertical axis is the height of the building, and the horizontal axes are the modification factors A_p (Figure 6a) and A_i (Figure 6b). As shown, when L_1/D is small the barrier is more effective in reducing the peak reflected

pressure and also impulse even though the duration of the positive phase of the blast pressure is longer (as shown in Figure5).

3.2 Building height effect

As the shock wave reaches the blast wall, a portion of the shock wave energy is reflected. The barrier also causes wave diffraction, and the diffraction process greatly weakens the shock wave energy locally behind the barrier. As a result, the maximum pressure may occur at a point higher than the blast wall on the building, although the reflection of the blast wave from the ground intensifies the blast pressure and thus results in a high peak reflected pressure at the building base. When building is low, a relatively large portion of the energy will propagate over the top of the building. This makes the pressure and impulse at the building base relatively low, as shown in the Figures 7 and 8 for the building height of 3m and 5m. Therefore, the peak reflected pressure distribution is sensitive to building hight when the building is relatively low.

To study the effectiveness of a blast wall on blast pressure reduction on buildings of different heights, numerical simulations corresponding to different building heights were carried out and the results compared. Typical ratios of the peak reflected pressure and impulse distribution along the height of different buildings are shown in Figure 7 and Figure 8 respectively. From both figures, it can be seen that: (1) when the building is lower than or comparable to $H_e(=H_1D/L_1$, where H_e is shown in Figure 1.*)*, the modification factors for both peak reflected pressure and impulse are generally smaller, especially when $L_1/D=0.8$; (2) once the building is higher than H_e, the modification factors are insensitive to the building heights except at a few points near the building top; (3) the modification factors for buildings higher than H_e all converge to that for the 20m building case, the highest building case considered in this study. Therefore, if the building is higher than H_e, the factors can be approximated to be the same as the values for the 20 m building. This assumption may result in a slightly conservative estimation of the factors for a relatively low building, especially at locations near its top.

3.3 Estimation of Peak Pressure and Impulse

Before the peak pressure and impulse distribution along the building height for the case with a barrier are estimated, the modification factor for the no barrier case need be determined first, because they serve

as the upper limit of the with barrier case as shown in Figure 6. For the no barrier case, the distribution factors can be obtained from available empirical methods, such as TM5-13 [11]. It is worth noting that, in the no barrier case, the maximum values for the peak reflected pressure and impulse always occur at the ground level, as shown in Figure 6.

From Figure 6, it is clear that the modification factors vary significantly along the building height. It can be found that in some curves there is a kink point with a local minimum value at about a few metres above the ground (The position of the kink point is marked in Figure 7.), while in other curves there is no obvious kink point. From the numerical results, it is found that when $(D-L_1)/H_1 \geq 4$, there is no kink point for A_i; and when $(D-L_1)/H_1 \geq 10$, there is no kink point for A_p. This observation indicates that local minimum appears if the distance between the barrier and building is small, and/or the barrier is high. Otherwise, no local minimum occurs and the maximum pressure and impulse occur at the ground level, and minimum at the building top.

To simplify the estimation of the modification factors along the building height, approximate piece-wise linear distribution is assumed as shown in Figure 9. For the cases with local minimum, four points need be determined. They are points A, B, C and D as shown in Figure 9a. To further simplify the estimation, it is assumed that Points A, C and D have the same modification factor, which is taken as the maximum modification factor along the building height. As shown in Figures 7 and 8, this assumption results in overestimation of the modification factors at some points along the building height. Numerical results indicated that the largest overestimation could be as high as 87.5%, corresponding to the case when L_1/D is large that the largest modification factor occurs at about the mid height of the building. Point B corresponds to the local minimum, and point D is the intersection point of the modification factors for the with-barrier and no barrier case. Above point D, the modification factor of the with-barrier case is assumed the same as the no barrier case. For the cases with no local minimum, only points A and D need be determined as shown in Figure 9 (b).

From the above simplification, one needs to determine the maximum and minimum modification factors A_{max} and A_{min} respectively for the reflected peak pressure and impulse, and the locations of points B and C since point A is at the ground level, and point D is just the intersection point of the A_{max} of the with-barrier case with that of the no barrier case. The maximum modification factors A_{max} can be

estimated as a function of three variables, namely, scaled distance $Z=D/W^{1/3}$ $(m/kg^{1/3})$, the ratio of the blast wall height to the distance between the explosion and the building H_1/D, the ratio of the distance between the blast wall and the explosion to that between the building and the explosion L_1/D. With least-squares method [18], the best fitted equations are as follows

$$A_{P\,max} = -0.1359 + (0.3272 + 0.1995\lg(H_1/D))\lg Z - 0.5626\lg(H_1/D) + 0.4666 L_1/D \quad (3)$$

$$A_{I\,max} = 0.0274 + (0.4146 + 0.2393\lg(H_1/D))\lg Z - 0.5044\lg(H_1/D) + 0.2538 L_1/D \quad (4)$$

R^2 statistics (multiple regression correlation coefficient, which gives the proportion of the variability of the response variable that is accounted for by the explanatory variable [18]) are calculated as 0.9026 and 0.9304 for the A_{Pmax} and A_{Imax}, respectively, implying that there is a good correlation between the variables. It should be noted that the values for both A_{Pmax} and A_{Imax} should be in the range from zero to one, therefore the above two equations are valid only in this range. Figure 10 and Figure 11 show the comparison of some results estimated from the above two equations with the numerical results of A_{Pmax} and A_{Imax}, respectively. The lines in the figures are the values obtained from Equation (3) or (4), while the scattered points are those obtained from numerical simulations. The maximum error between the fitted equations and the scattered points for A_{Pmax} and A_{Imax} is 49% and 38% respectively.

The position and the relative value of the local minimum (point B) are also analysed and the simplified formulae are obtained. With least squares fitting, the best equations for point B are

$$(H_{P\min} - H_1)/D = -0.4275 + 0.0366\lg Z - 0.4043\lg(H_1/D) - 0.1709\lg(L_1/D) \quad (5)$$

$$A_{P\,min}/A_{P\,max} = -0.0284 + 0.244\lg Z - 0.4302\lg(H_1/D) - 0.3475\lg(L_1/D) \quad (6)$$

$$(H_{I\min} - H_1)/D = -0.2474 + 0.1084\lg Z - 0.2450\lg(H_1/D) - 0.2377\lg(L_1/D) \quad (7)$$

$$A_{I\,min}/A_{I\,max} = 0.3196 + 0.2154\lg Z - 0.3173\lg(H_1/D) - 0.2013\lg(L_1/D) \quad (8)$$

where H_{Pmin} is the position of point B for the pressure, as shown in Figure 9(a), A_{Pmin} is for the local minimum pressure; similarly, H_{Imin} is the position of point B for the impulse, A_{Imin} is for the local minimum impulse. R^2 statistics for Equations (5) to (8) are, 0.7261, 0.9109, 0.6356 and 0.8153, respectively.

The position of point C is also determined from least squares fitting of the numerical data, as

$$H_{P\max}/D = 1.0995 - 0.0105\lg Z + 0.7806\lg(H_1/D) - 0.4109\lg(L_1/D) \quad (9)$$

$$H_{\mathrm{I}max} / D = 1.1994 - 0.0843 \lg Z + 0.8329 \lg(H_1 / D) - 0.1841 \lg(L_1 / D) \quad (10)$$

where H_{Pmax} is position C for pressure, and H_{Imax} is for impulse. R^2 statistics are 0.8203 and 0.7353, respectively.

4 Arrival Time and positive phase duration

Typical reflected pressure-time history is shown in figure 12. It is characterized by a sudden pressure rise to the peak value at the shock front, and followed by a decrease back to ambient pressure and then a negative phase. The parameters needed to model the shock wave time history include the shock wave front arrival time T_a, peak reflected pressure P_r, impulse I_r, and the positive phase duration T_0. It should be noted that in some cases when the gauge point is behind the barrier, the positive phase may have two impulses due to the reflection caused by the barrier, as shown in Figure 5(b). In the present study, the peak reflected pressure for the second pulse is not considered specifically but is included in the evaluation of the positive impulse and duration.

4.1 Estimation of arrival time

Using the simulated pressure time histories, the arrival time of the front wave can be extracted. With the least squares fitting, the best fitted equation for arrival time is as follows

$$\lg(T_a / W^{1/3}) = \begin{cases} -0.0921 + 1.4806 \lg Z + 0.1388 \lg(H_1 / D) - 0.0551 \lg(L_1 / D) + 0.008H, & H \geq H_e \\ -0.0921 + 1.4806 \lg Z + 0.1388 \lg(H_1 / D) - 0.0551 \lg(L_1 / D) + 0.008H_e, & H < H_e \end{cases} \quad (11)$$

where T_a is arrival time (ms), H is gauge point height. R^2 statistics is 0.9603. Figure 13 shows the comparison of some results estimated from Equation (11) with the numerical results. It can be seen that the approximate lines match the numerical results very well.

4.2 Estimation of positive phase duration

The blast wave arrives at a given location at time T_a and, after rise to the peak value, the pressure decays to the ambient value in time to which is the positive phase duration T_0 [11]. The best–fitted relation between the positive phase duration T_0 and the other parameters is

$$\lg(T_0 / W^{1/3}) = 0.1699 + 0.9274 \lg Z + 0.1154 \lg(H_1 / D) - 0.0793 \lg(L_1 / D) - 0.0022H \quad (12)$$

R^2 statistics is 0.9254. Figure 14 shows comparisons of numerical results with the approximate formula (12).

5 Reflected Pressure-time History

For design purpose, it is necessary to establish the variation of the pressure with time since blast effects on structures depend on the pressure-time history. In the present study, the pressure-time history is approximated by two fictitious triangular pressure pulses, namely, a positive pulse and a negative pulse (as shown in Figure 12).

5.1 Positive phase pressure-time history

The actual positive phase duration is replaced by a fictitious duration, which is estimated from the total positive impulse and peak pressure as

$$T_{of} = 2I / P_r \tag{13}$$

where I and P_r are determined by multiplying the corresponding impulse and peak pressure from the no barrier case by the modification factors. Impulse and peak pressure corresponding to the no barrier case can be estimated from many empirical formulae, such as those given in TM5-1300 [11]. Other parameters, such as, T_a *and* T_0, can be obtained using the approximate formulae derived in the previous sections.

5.2 Negative phase pressure-time history

Numerical results show that the blast wall has little effect on the negative phase of the pressure (Figure 5). Therefore, available empirical formulae for the negative phase blast pressure for the no barrier case can be used. For determining the pressure-time data for the negative phase, the same method as that in TM5-1300 is employed in the present study. The equivalent negative phase pressure-time curve will have a rise time equal to 0.25 of the fictitious duration T_{of}^-, which is given by the triangular equivalent pulse duration,

$$T_{of}^- = 2I^- / P_r^- \tag{14}$$

where I^- and P_r^- are the impulse and peak pressure of the negative phase for the no barrier case, which can be determined from TM5-1300.

It should be noted that, as discussed above, in some cases the blast load may damage the barrier. However, this is not considered in the present study. Further research work will be carried out to include possible barrier damage in numerical modelling and simulation.

6 Application examples

Example 1: the TNT equivalent charge weight *W=300kg*, distance from charge to the building *D=10m*, the height of the building H_B*=10m*, the blast wall height H_1*=2m*, the distance between the blast wall and the explosion L_1*=4m*, determine the peak reflected pressure and impulse along the building height, and the arrival time and positive phase duration of a gauge point on building surface at 5 m above the ground level.

Step 1: calculate the scaled distance *Z*,

$$\mathrm{Z} = \mathrm{D}/\mathrm{W}^{1/3} = 10/300^{1/3} = 1.4938 m/kg^{1/3}$$

Step 2: estimate the peak reflected pressure $P_{no\_barrier}$ and impulse $I_{no\_barrier}$ at the ground level on the building front surface for the no barrier case from TM5-1300 or other empirical formulae,

At ground level, $P_{no\_barrier}$*=2.5627MPa*, $I_{no\_barrier}$*=3.5052MPa·ms*. Their distributions along the building height are shown in Figure 15.

Step 3: check if there is a local minimum for A_p and A_i,

$$(D - L_1)/H_1 = 3$$

It is less than 4, which means that there is local minimum for both A_p and A_i.

Step 4: calculate the maximum modification factors A_{pmax} and A_{imax} from Eq (3) and (4), then obtain the maximum peak reflected pressure P_{max} and impulse I_{max},

$$\begin{aligned} A_{p\max} &= -0.1359 + (0.3272 + 0.1995\lg(2/10))\lg 1.4938 - 0.5626\lg(2/10) + 0.4666 \times 4/10 \\ &= 0.4767 \end{aligned}$$

$$A_{i\max} = 0.0274 + (0.4146 + 0.2393\lg(2/10))\lg 1.4938 - 0.5044\lg(2/10) + 0.2538 \times 4/10 = 0.5246$$

$$P_{\max} = A_{p\max} \times P_{no\_barrier} = 0.4767 \times 2.5627 = 1.2216 MPa$$

$$I_{\max} = A_{i\max} \times I_{no\_barrier} = 0.5246 \times 3.5052 = 1.8388 MPa \cdot ms$$

Step 5: calculate the H_{Pmin}, P_{min}, H_{Imin}, I_{min}, H_{Pmax}, H_{Imax} from Eqs (5)-(10),

$$(H_{P\min} - H_1)/D = -0.4275 + 0.0366\lg 1.4938 - 0.4043\lg(2/10) - 0.1709\lg(4/10) = -0.0705$$

$$P_{\min}/P_{\max} = A_{p\min}/A_{p\max}$$
$$= -0.0284 + 0.244\lg 1.4938 - 0.4302\lg(2/10) - 0.3475\lg(4/10) = 0.4531$$

$$(H_{\mathrm{Im}in} - H_1)/D = -0.2474 + 0.1084\lg 1.4938 - 0.2450\lg(2/10) - 0.2377\lg(4/10) = 0.0373$$

$$I_{\min}/I_{\max} = A_{i\min}/A_{i\max}$$
$$= 0.3196 + 0.2154\lg 1.4938 - 0.3173\lg(2/10) - 0.2013\lg(4/10) = 0.6590$$

$$H_{P\max}/D = 1.0995 - 0.0105\lg 1.4938 + 0.7806\lg(2/10) - 0.4109\lg(4/10) = 0.7156$$

$$H_{\mathrm{Im}ax}/D = 1.1994 - 0.0843\lg 1.4938 + 0.8329\lg(2/10) - 0.1841\lg(4/10) = 0.6758$$

Thus, $H_{pmin}=1.2948m$, $P_{min}=0.5535MPa$, $H_{Imin}=2.3733m$, $I_{min}=1.2118MPa{\cdot}ms$, $H_{Pmax}=7.156m$, $H_{Imax}=6.758m$. Peak pressure and impulse distribution are then obtained as shown in Figure 15. From the figure, it can be found that when H is equal to 5m, the peak pressure and the impulse are 0.9758MPa and 1.5874MPa·ms, respectively.

Step 6: calculate the arrival time and the positive duration from Eq (11) and (12)

$$\lg(T_a/W^{1/3}) = -0.0921 + 1.4806\lg 1.4938 + 0.1388\lg(2/10) - 0.0551\lg(4/10) + 0.008 \times 5 = 0.1309$$

$$\lg(T_0/W^{1/3}) = 0.1699 + 0.9274\lg 1.4983 + 0.1154\lg(2/10) - 0.0793\lg(4/10) - 0.0022 \times 5 = 0.2714$$

Accordingly, $T_a=9.05ms$, $T_0=12.50ms$.

Step 7: obtain the fictitious positive duration and the simplified triangular positive phase

$$T_{of} = 2I/P_r = 2 \times 1.5874/0.9758 = 3.2535ms$$

Example 2: the TNT equivalent charge weight $W=1000kg$, the distance from charge to the building $D=50m$, the height of the building $H_B=20m$, the blast wall height $H_1=1m$, the distance between the blast

wall and the explosion $L_1=10m$, determine the peak pressure and impulse distribution along the building height.

Step 1: calculate the scaled distance *Z*,

$$\mathrm{Z} = \mathrm{D}/\mathrm{W}^{1/3} = 50/1000^{1/3} = 5m/kg^{1/3}$$

Step 2: estimate the peak reflected pressure $P_{no\_barrier}$ and impulse $I_{no\_barrier}$ at the ground level on the building front surface for the no barrier case from TM5-1300 or other methods,

At ground level, $P_{no\_barrier}=0.1MPa$, $I_{no\_barrier}=1.25MPa\cdot ms$.

Step 3: Check if there is a local minimum for A_p and A_i

$$(D - L_1)/H_1 = (50-10)/1 = 40$$

It is greater than 10, which means that there is no local minimum for either A_p nor A_i.

Step 4: calculate the maximum modification factors A_{pmax} and A_{imax} from Eq (3) and (4), then obtain the maximum peak reflected pressure P_{max} and impulse I_{max},

$$A_{p\,max} = -0.1359 + (0.3272 + 0.1995\lg(1/50))\lg 5 - 0.5626\lg(1/50) + 0.4666\times 10/50 = 0.9051$$

$$A_{i\,max} = 0.0274 + (0.4146 + 0.2393\lg(1/50))\lg 5 - 0.5044\lg(1/50) + 0.2538\times 10/50 = 0.9407$$

$$P_{\max} = A_{p\max}\times A_{no\_barrier} = 0.9051\times 0.1 = 0.0905MPa$$

$$I_{\max} = A_{i\max}\times I_{no\_barrier} = 0.9407\times 1.25 = 1.1759MPa\cdot ms$$

Peak pressure and impulse distribution are then obtained as shown in Figure 16.

7 Conclusions

Numerical simulations were carried out to study the effectiveness of blast barriers for blast load reduction. It was found that a barrier between an explosion and a building can not only reduce the peak reflected pressure and impulse on the surface of the building, but also delay the arrival time of the blast wave. The effectiveness of a blast barrier in reducing the blast pressure on structures behind the barrier

depends not only on the barrier height, distances between the explosion center and barrier, distance between the barrier and structure, but also on the structure height.

Based no the numerical results, approximate formulae have been derived to estimate the reflected pressure-time history on a structure behind a barrier. Those formulae, used together with other available empirical methods (such as TM5-1300) provide a simple and reliable estimation of blast loading on building structures behind a blast barrier.

Acknowledgements

The authors would like to thank the Australian Research Council for partial financial support under grant no. DP0451966 for carrying out this research work.

References

[1] Ambrosini, D., Luccioni, B, Jacinto, A. and Danesi, R. Location and mass of explosive from structural damage. Engineering Structures, 2005; 27:167-176.

[2] Remennikov, A. M. and Rose, T. A. Modelling blast loads on buildings in complex city geometries. Computers and Structures, 2005; 83(27):2197-2205.

[3] Luccioni, B.M., Ambrosini, R.D. and Danesi, R.F. Analysis of building collapse under blast loads. Engineering Structures. 2004; 26:63-71.

[4]Longinow, A. and Mniszewski, K. R. Protecting building against vehicle bomb attacks. Practice Periodical on Structures, ASCE, 1996; 1(1):51-54.

[5] Rose, T.A., Smith, P.D. and Mays, G.C. The effectiveness of walls designed for the protection of structures against airblast from high explosives. Proceedings of the Institution of Civil Engineers-Structures and Buildings. 1995; 110(1):78-85.

[6] Rose, T.A., Smith, P.D. and Mays, G.C. Design charts relating to protection of structures against airblast from high explosives. Proceedings of the Institution of Civil Engineers-Structures and Buildings. 1997; 122(2):186-192.

[7] Rose, T.A., Smith, P.D. and Mays, G.C. Protection of structures against airblast using barriers of limited robustness. Proceedings of the Institution of Civil Engineers-Structures and Buildings. 1998; 128(2):167-176.

[8] Bogosian, D. and Piepenburg, D. Effectiveness of frangible barriers for blast shielding. Proceedings of the 17th International Symposium on the Military Aspects of Blast and Shock, Las Vegas, Nevada, 2002; p.1-11.

[9] Ngo, T., Nguyen, N. and Mendis, P. An investigation on the effectiveness of blast wall and blast-structure interaction. Development in Mechanics of Structures and Materials, Proceedings of the 18th Australia Conference on the Mechanics of Structures and Materials, Perth, Australia, 2004; p.961-967.

[10] Zhou, X. Q. and Hao, H. Numerical Analysis of the effectiveness of Barriers for Blast Shielding. The Ninth International Symposium on Structural Engineering for Young Experts, August 18-21 2006, Fuzhou & Xiamen, China. 2006; 1134-1139.

[11] TM5-1300. Structures to resist the effects of accidental explosions. US Department of the army. USA, 1990.

[12] Henrych, J. The Dynamics of Explosion and its Use. Elsevier Amsterdam, 1979.

[13] Chapman, T.C., Rose, T. A. and Smith, P.D. Blast wave simulation using AUTODYN2D: a Parametric Study. International Journal of Impact Engineering. 1995; 16(5/6):777-787.

[14] Wu, C and Hao, H. Modelling of simultaneous ground shock and airblast pressure on nearby structures from surface explosions. International Journal of Impact Engineering, 2005; 31:699-717.

[15] Wu, C, Lu, Y, Hao, H. Numerical prediction of blast-induced stress wave from large-scale underground explosion. International Journal for Numerical and Analytical Methods in Geomechanics, 2004; 28(1): 93-109.

[16] AUTODYN. Century Dynamics, Theory manual. 2003.

[17] Zhou, X.Q., Hao, H. and Deeks, A. J. Numerical simulation of blast wave propagation in a building structure. The 4th homeland security summit and exposition, Science, engineering and technology summit on counter-terrorism technology. Canberra, Australia, 14 July, 2005; p.83-96.

[18] Kottegoda, N.T., and Rosso, R. Statistics, Probability, and Reliability for Civil and Environmental Engineers. McGraw-Hill Companies, New York Inc. 1997.

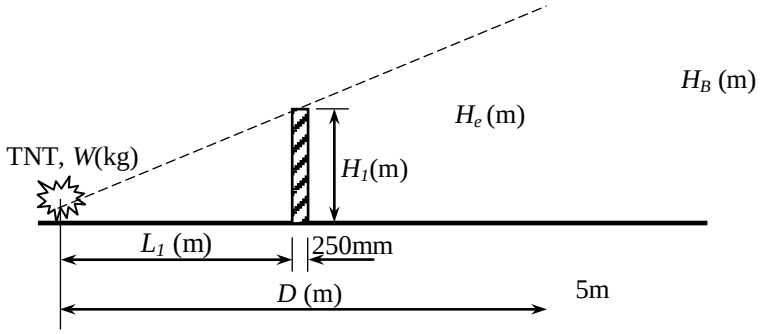

Figure 1. Problem Configuration

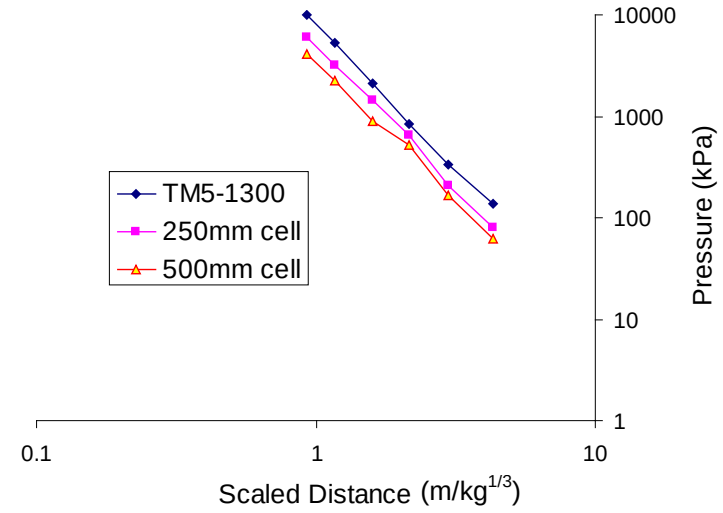

(a) Peak reflected pressure

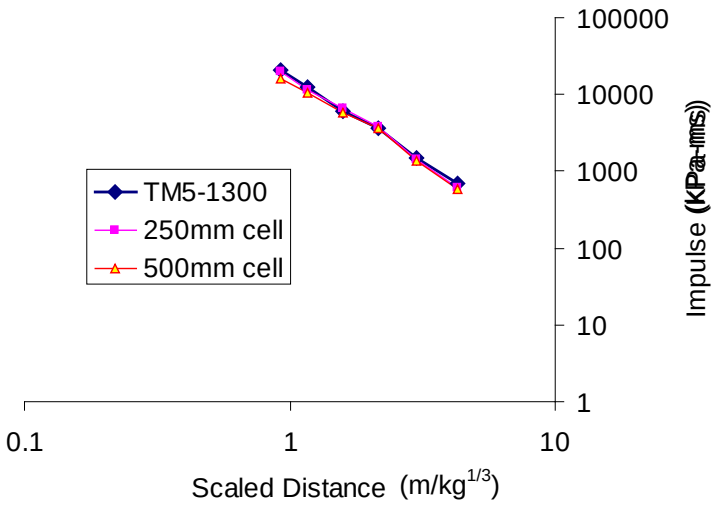

(b) Impulse

Figure 2. Peak reflected pressure and impulse for different scaled distances (H_B=20m, D=20m)

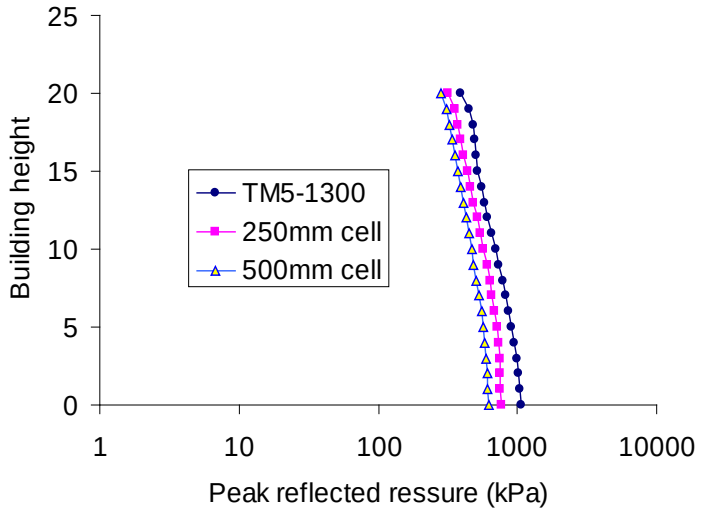

(a) Peak reflected pressure

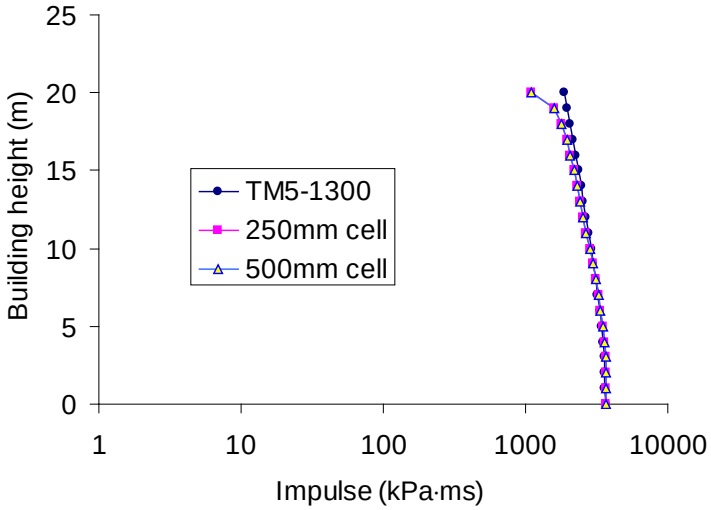

(b) Impulse

Figure 3. Peak reflected pressure and impulse along building height (H_B=20m, D=20m, W=1000kg)

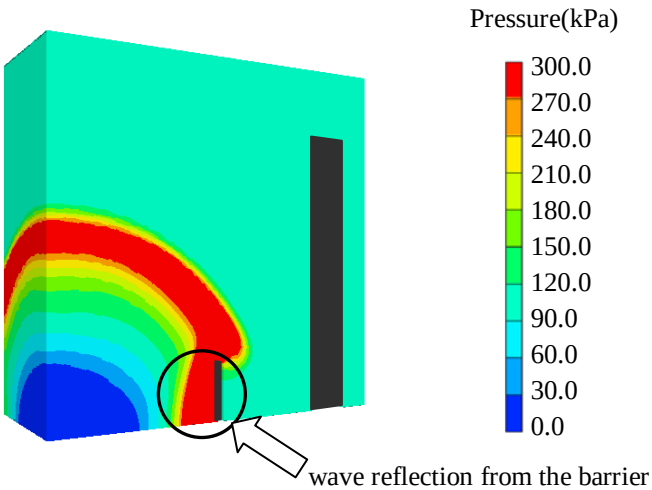

(a) t=10ms

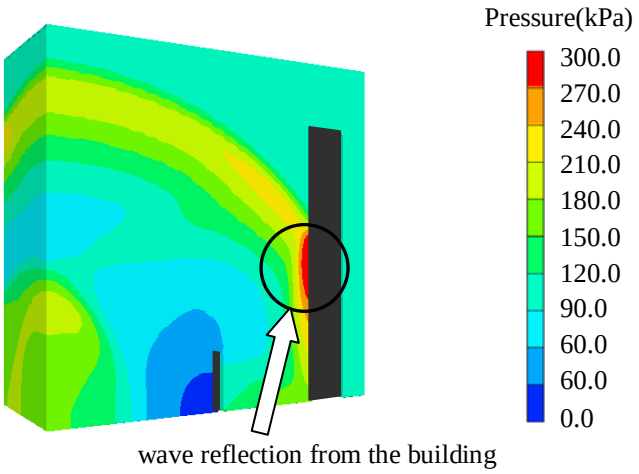

(b) t=25ms

Figure 4. Pressure wave propagation

(*H_B=20m, H_1=4m, D=20m, W=1000kg, L_1/D=0.6*)

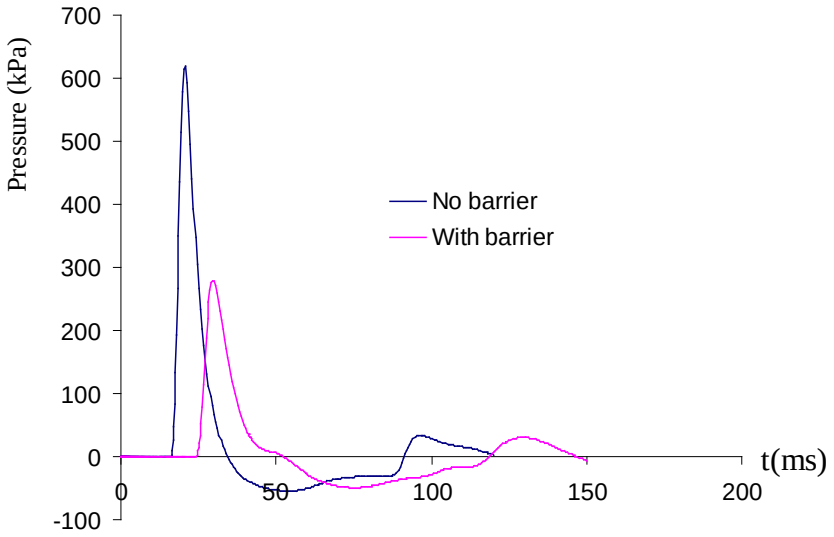

(a) gauge point at *H=0m*

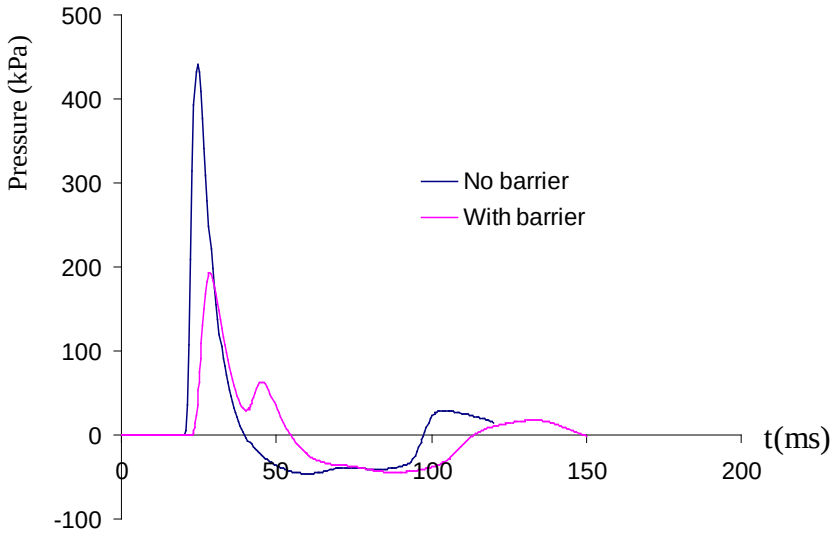

(b) gauge point at *H=10*m

Figure 5. Reflected pressure time history at different gauge points

(H_B=*20m*, H_1=*2.5m*, *D=20m*, *W=1000kg*, L_1/D=*0.2*)

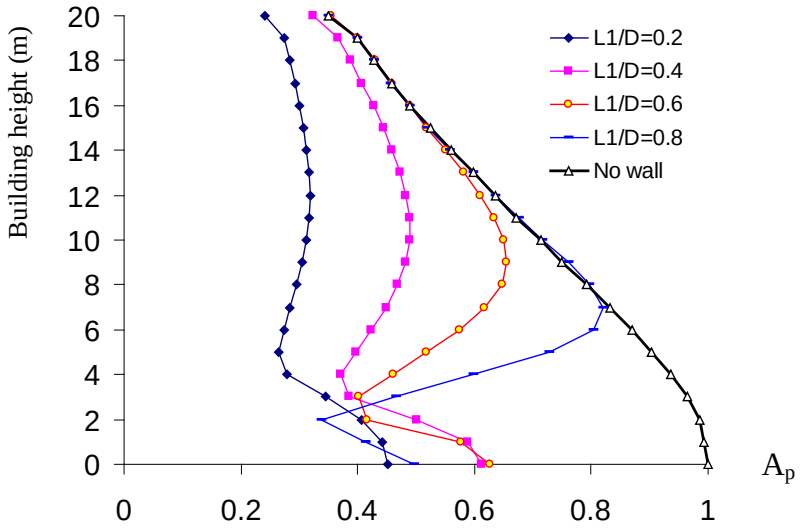

(a) peak reflected pressure

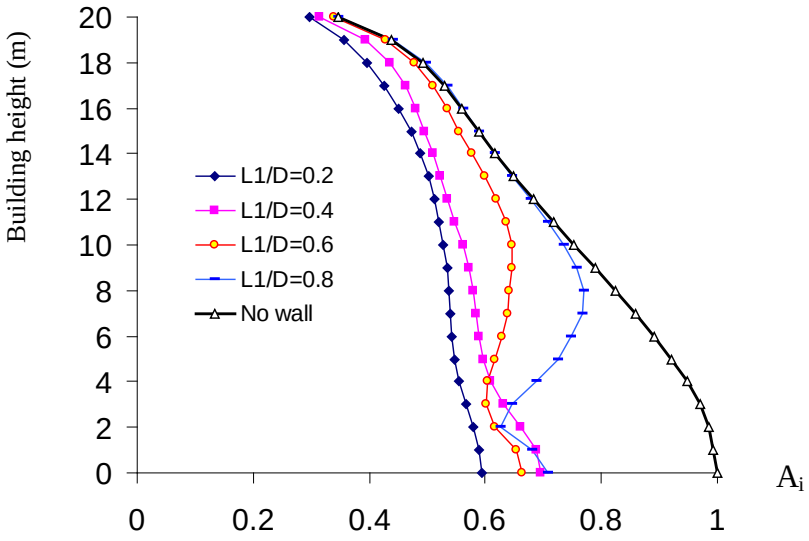

(b) impulse

Figure 6. Modification factors for peak reflected pressure and impulse versus building height

(H_B=20m, H_1=2.5m, D=20m, W=1000kg)

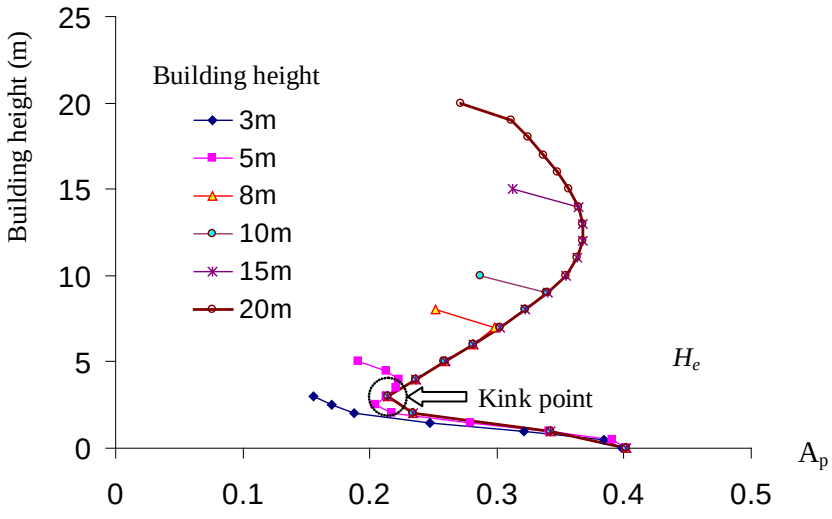

(a) $L_1/D=0.4$

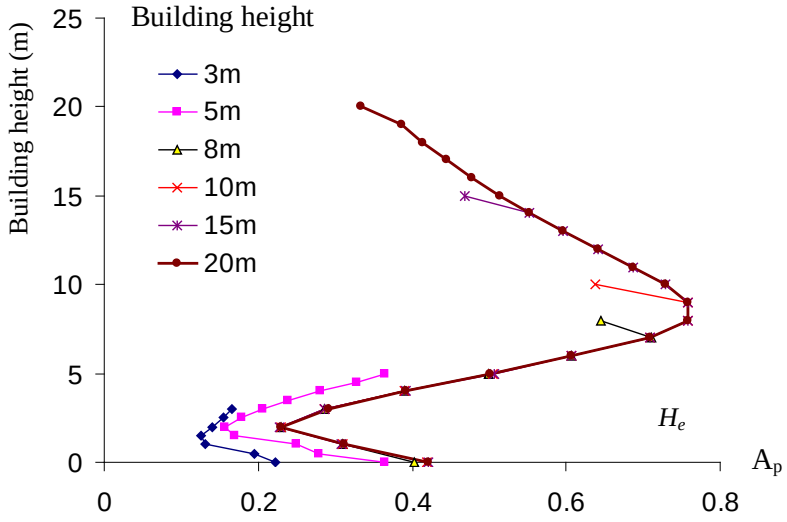

(b) $L_1/D=0.8$

Figure 7. Modification factors A_p for buildings with different heights

($H_1=4m$, $D=20m$, $W=1000kg$)

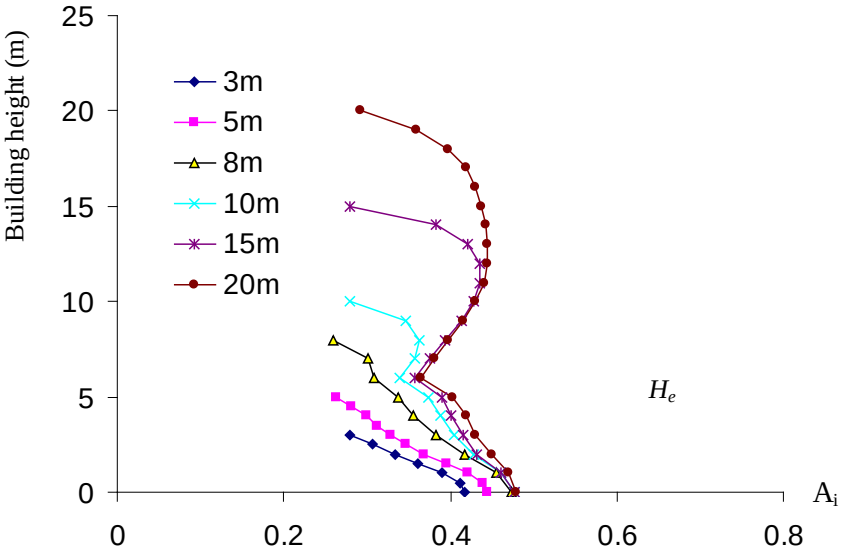

(a) $L_1/D=0.4$

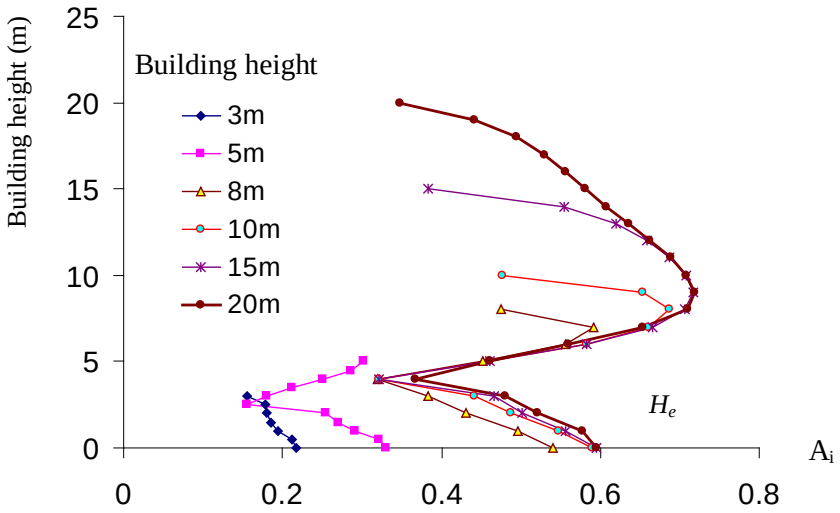

(b) $L_1/D=0.8$

Figure 8. Modification factors A_i for buildings with different heights

($H_1=4m$, $D=20m$, $W=1000kg$)

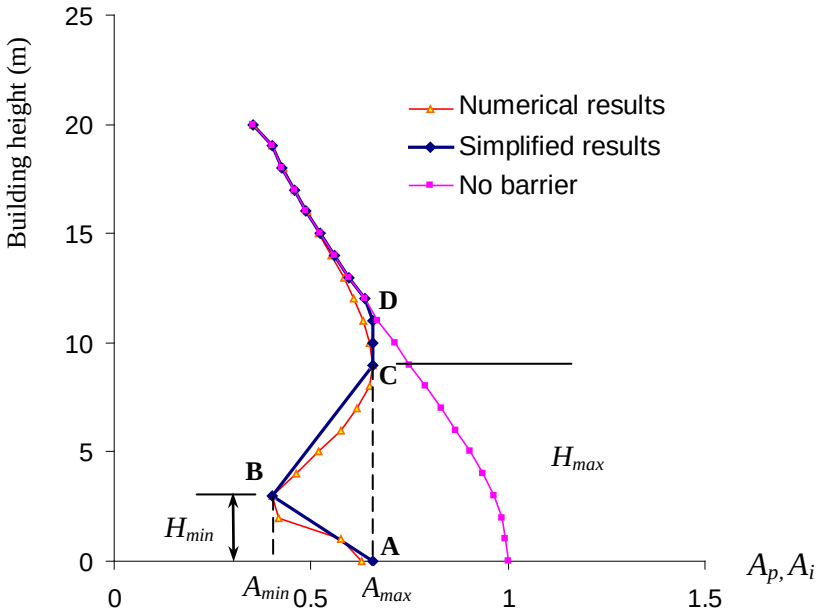

(a) H_B=20m, H_1=2.5m, L_1=12m, D=20m, W=1000kg

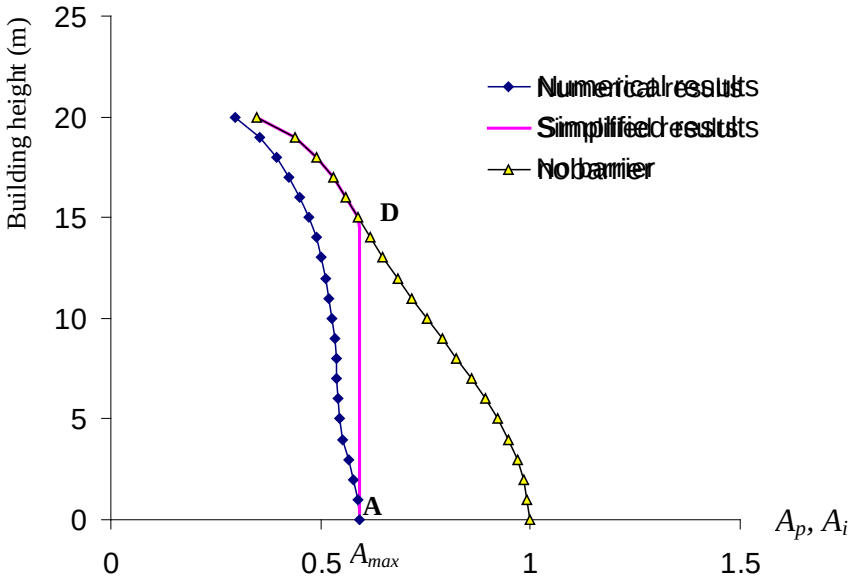

(b) H_B=20m, H_1=2.5m, L_1=4m, D=20m, W=1000kg

Figure 9 Simplified distribution of A_p and A_i along the building height

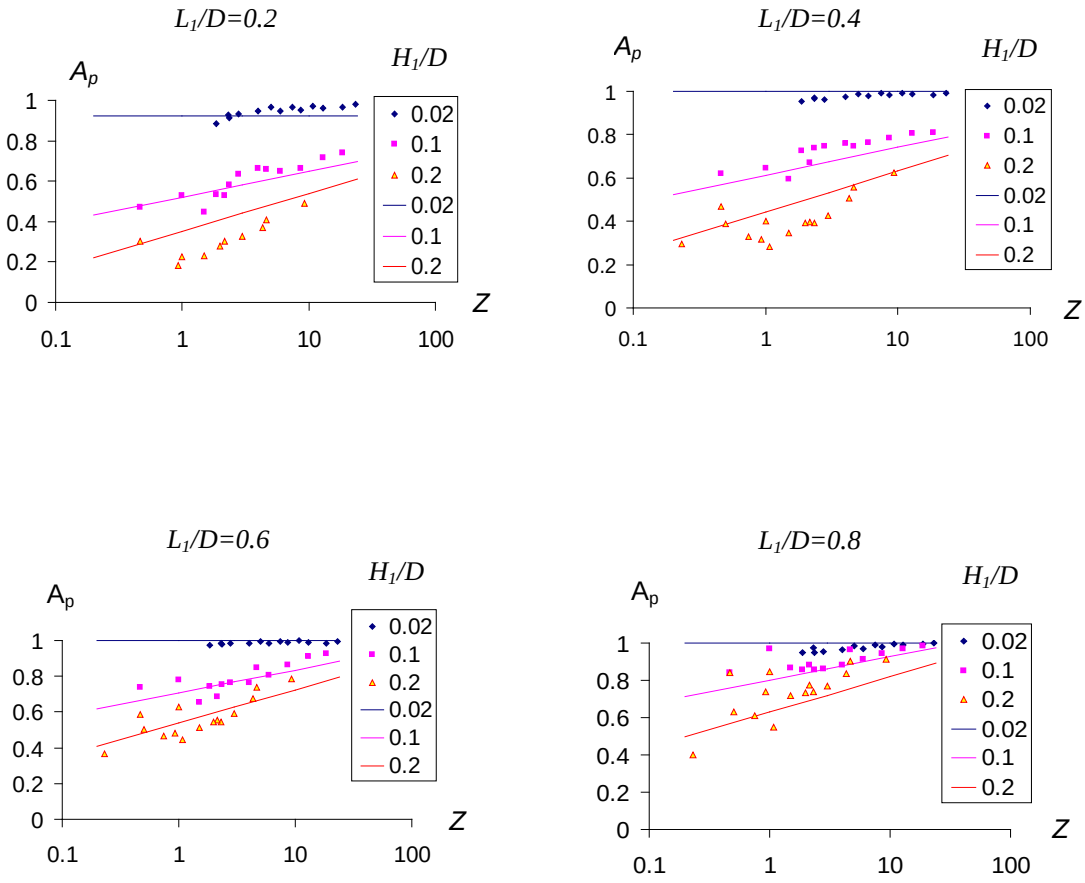

Figure 10 Comparison of the approximate results with the numerical results for A_p

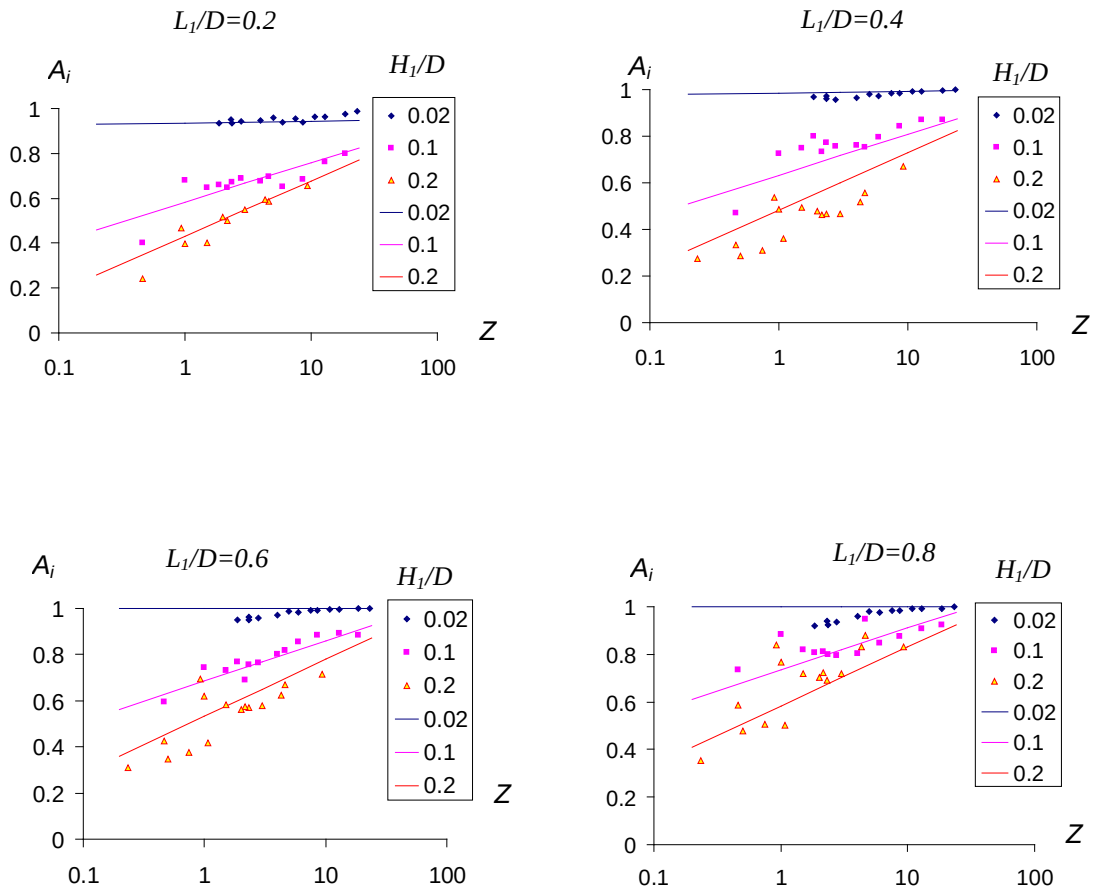

Figure 11 Comparison of the approximate results with the numerical results for A_i

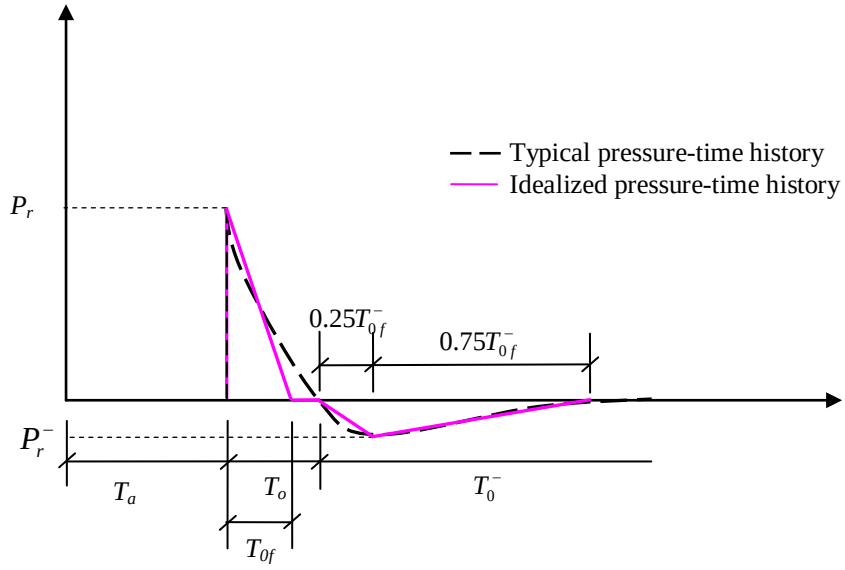

(a) single pulse

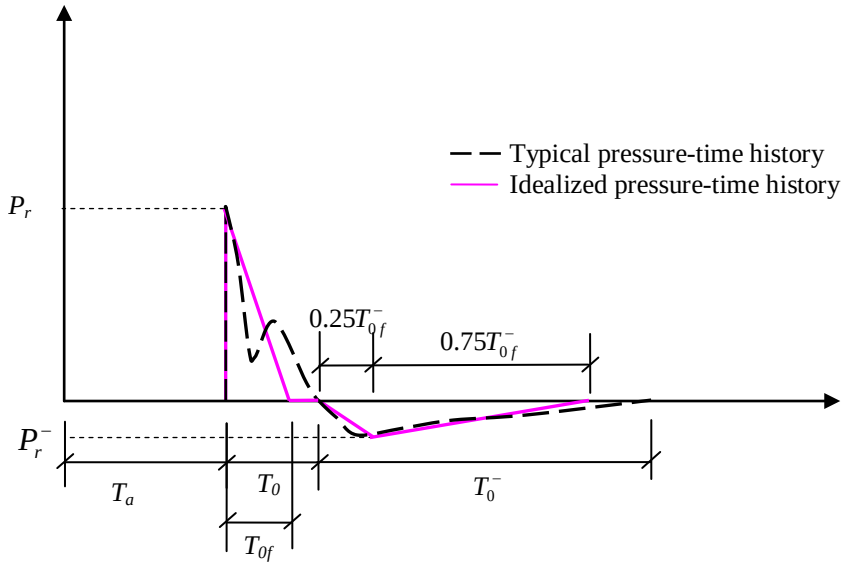

(b) two pulses

Figure 12. Typical reflected pressure-time history

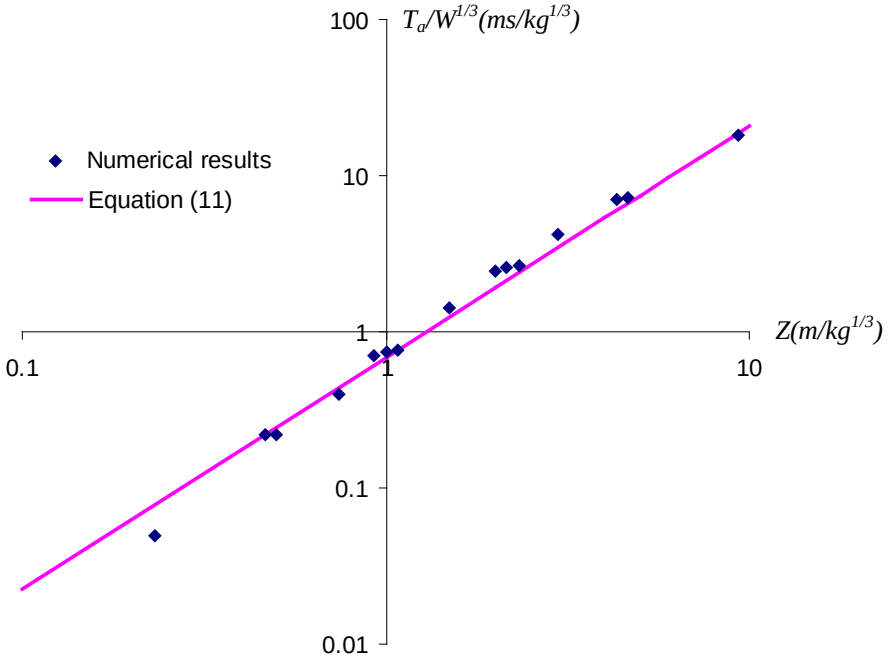

(a) $H_1/D=0.2$, $L_1/D=0.4$, $H=0$

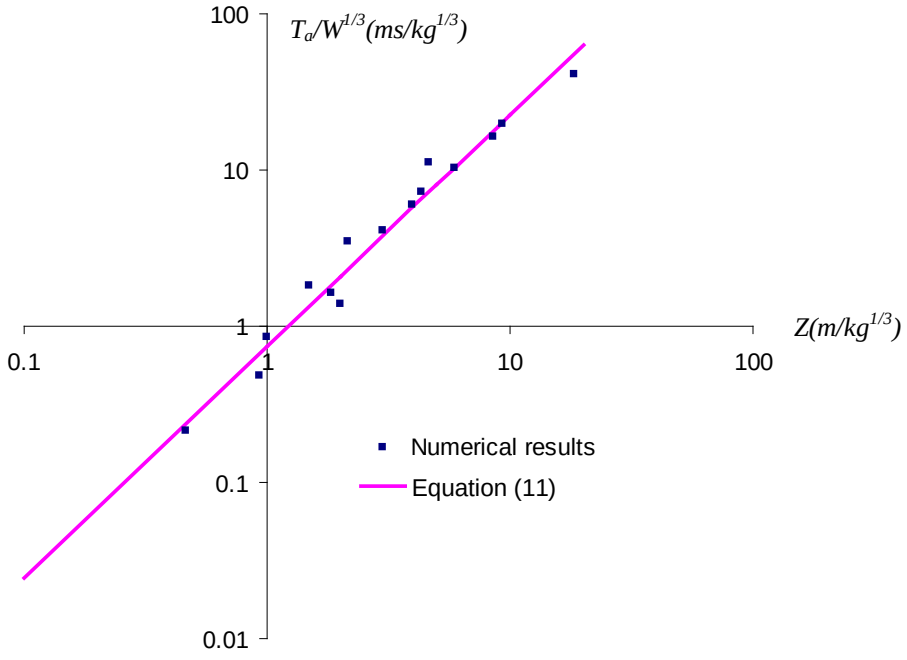

(b) $H_1/D=0.1$, $L_1/D=0.4$, $H=10$

Figure 13**.** Comparison of the approximate results with the numerical results for arrival time T_a

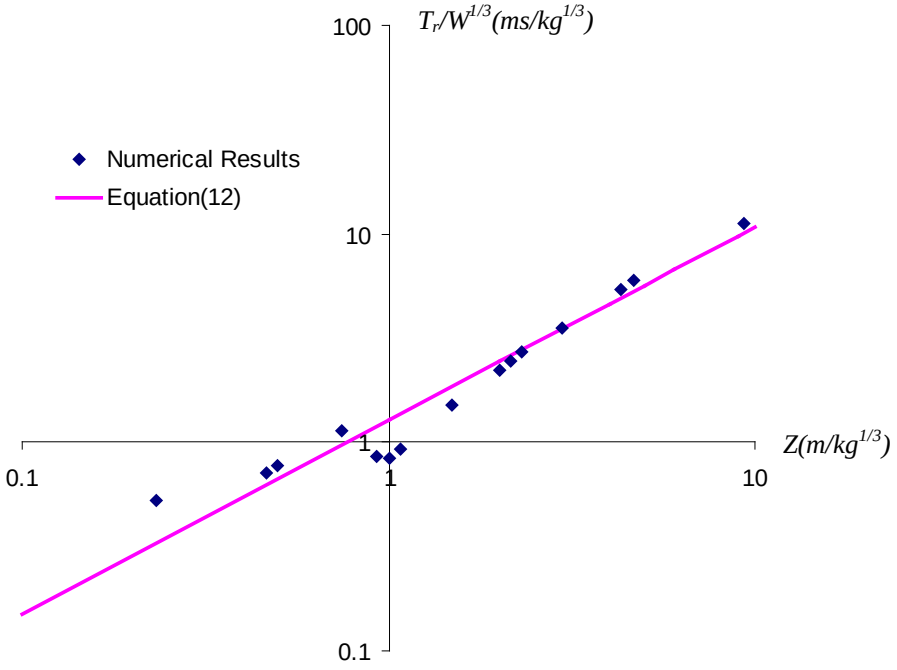

(a) $H_1/D=0.2$, $L_1/D=0.6$, $H=0$

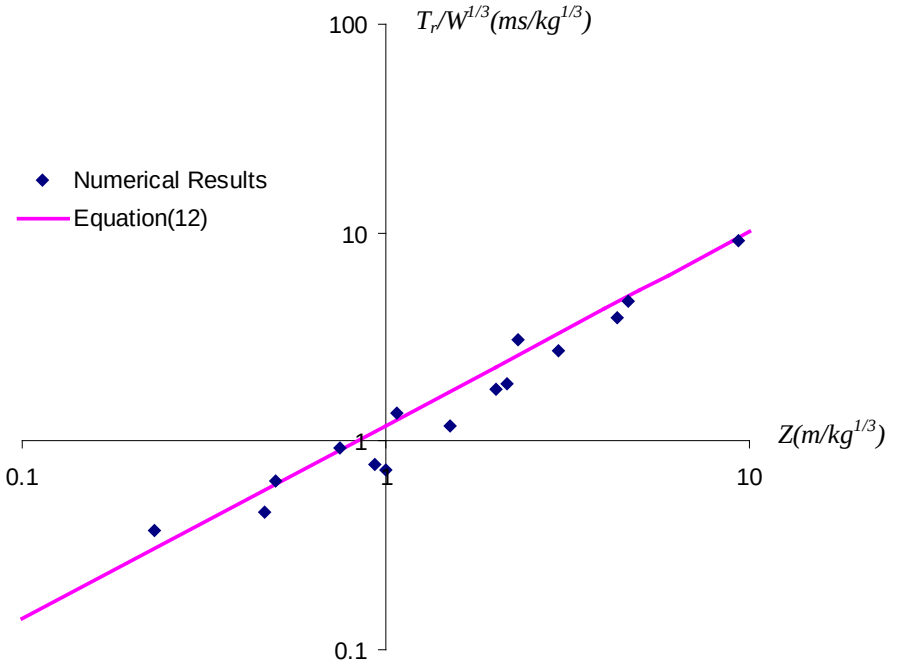

(b) $H_1/D=0.2$, $L_1/D=0.8$, $H=10$

Figure 14**.** Comparison of the approximate results with the numerical results for positive phase duration T_0

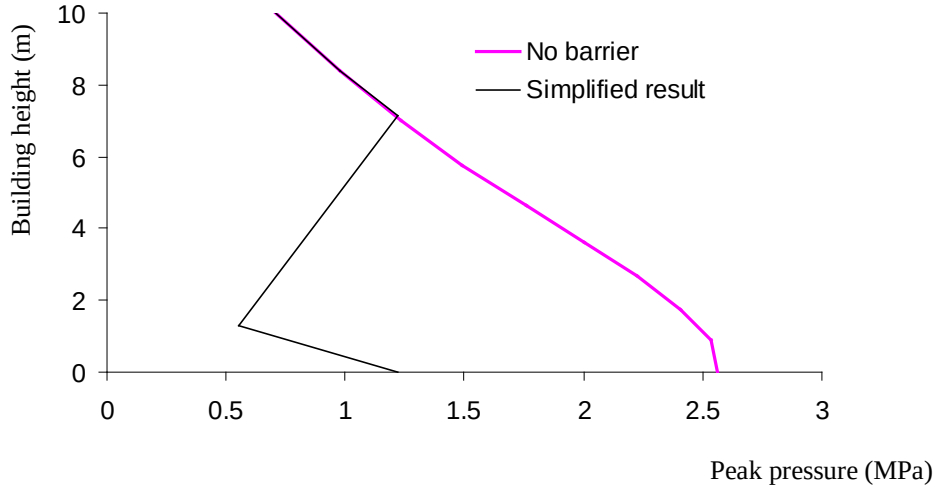

(a) Pressure

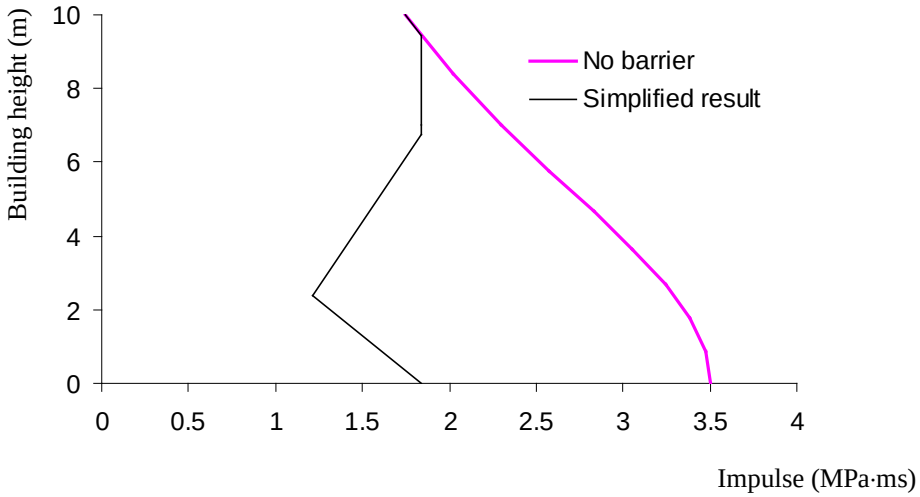

(b) Impulse

Figure 15. Estimated peak pressure and impulse distribution for example 1

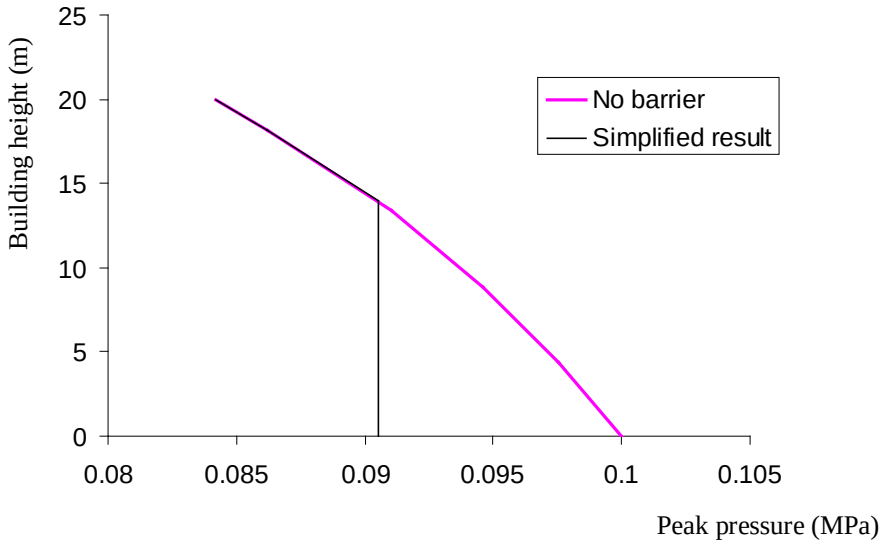

(a) Pressure

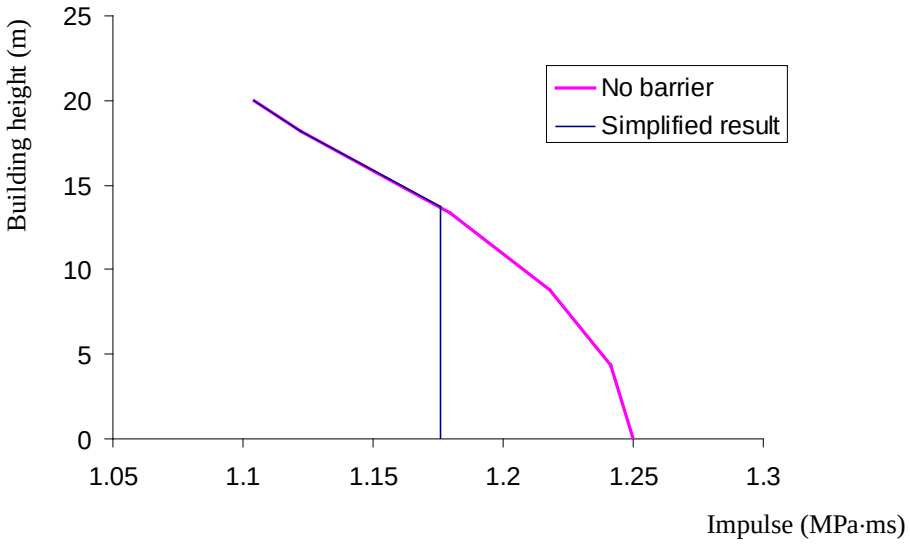

(b) Impulse

Figure 16. Estimated peak pressure and impulse distribution for example 2